From Substrate to Fragments to Inhibitor Active In Vivo against Staphylococcus aureus

Muriel Gelin, Julie Paoletti, Marie-Anne Nahori, Valeŕie Huteau, Clarisse Leseigneur, Gregory Jouvion, Laurence Dugué, David Clément, Jean-Luc Pons, Liliane Assairi, et al.

ACS Infectious Diseases

pubs.acs.org/journal/aidcbc

Article

From Substrate to Fragments to Inhibitor Active *In Vivo* against *Staphylococcus aureus*

Muriel Gelin,[¶] Julie Paoletti,[¶] Marie-Anne Nahori,[¶] Valérie Huteau,[¶] Clarisse Leseigneur, Grégory Jouvion, Laurence Dugué, David Clément, Jean-Luc Pons, Liliane Assairi, Sylvie Pochet,* Gilles Labesse,* and Olivier Dussurget*

Cite This: https://dx.doi.org/10.1021/acsinfecdis.9b00368

Read Online

ACCESS | Metrics & More | Article Recommendations | Supporting Information

ABSTRACT: Antibiotic resistance is a worldwide threat due to the decreasing supply of new antimicrobials. Novel targets and innovative strategies are urgently needed to generate pathbreaking drug compounds. NAD kinase (NADK) is essential for growth in most bacteria, as it supports critical metabolic pathways. Here, we report the discovery of a new class of antibacterials that targets bacterial NADK. We generated a series of small synthetic adenine derivatives to screen those harboring promising substituents in order to guide efficient fragment linking. This led to NKI1, a new lead compound inhibiting NADK that showed *in vitro* bactericidal activity against *Staphylococcus aureus*. In a murine model of infection, NKI1 restricted survival of the bacteria, including methicillin-resistant *S. aureus*. Collectively, these findings identify bacterial NADK as a potential drug target and NKI1 as a lead compound in the treatment of staphylococcal infections.

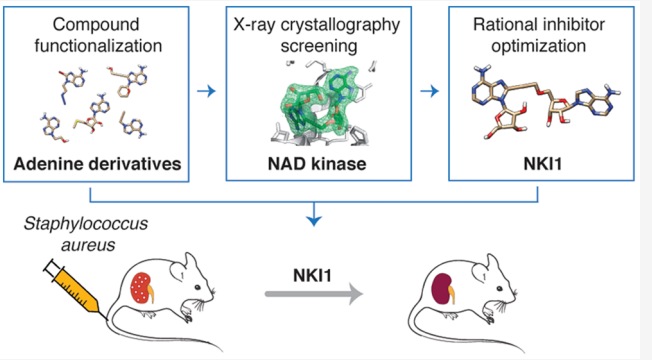

KEYWORDS: *adenosine derivative, bacterial NAD kinase, antibacterial compound, staphylococci, MRSA*

Methods for rapid design and synthesis of new antimicrobial compounds are eagerly sought to battle pathogens and cure infectious diseases.[1] Despite a vast repertoire of methods, quicker routes are still necessary to keep pace with the fast emergence of antibiotic resistance in pathogens. Similarly, the failure of major antibiotic classes calls for rapid identification of novel targets to produce the next generation of anti-infectious agents. NAD kinases (NADKs) have a central role in oxido-reductive functions but are still lacking a quality inhibitor although their important biochemical activity has been known for decades.[2] The genes encoding the NADKs were discovered by genomic analysis two decades ago,[3] and they were shown to be essential for growth in many bacterial species.[4−6] Interestingly, NADKs belong to a small and particular superfamily of kinases very distantly related to any other NAD or ATP binding proteins.[7] Indeed, they harbor a two-domain organization made of small alpha/beta fold and an all-beta domain, distantly related only to two lipid kinases existing in humans.[7] Not only is the fold unique, but also the particular conformation of the NAD in their binding site brings the two ribose moieties in close proximity (distance: ∼4 Å). This distance is much longer (∼7 Å) in other NAD(P) binding sites.[8] This suggested that NADKs represent promising targets and that specific inhibitors could be designed.

Fragment-based drug design (FBDD) is an attractive method for the rapid discovery of starting points to design new lead compounds. It relies on screening very small molecules, usually with millimolar affinity. Their small size allows an exhaustive diverse search with a few molecules (10^2 to 10^4 molecules) within the corresponding chemical space (an estimated 10^7 molecules).[9] This rational approach has already produced new ligands with affinities in the nanomolar range for several targets,[10] and yielded three clinical drugs. However, fragment optimization to build higher affinity binders, and particularly fragment linking, is still not straightforward,[10] despite the seminal discovery of high affinity inhibitors of the FK506 binding protein and additional attempts since then.[11−13] In theory,[14] perfect linking of two or three fragments with an expected low millimolar affinity for a target should provide new compounds with low micromolar or nanomolar activity and hence a rapid route toward a promising lead compound, but this is rarely achieved. Currently, there is no single method to efficiently guide the connection of selected fragments, which requires both affinity estimates and

Received: September 25, 2019
Published: February 4, 2020

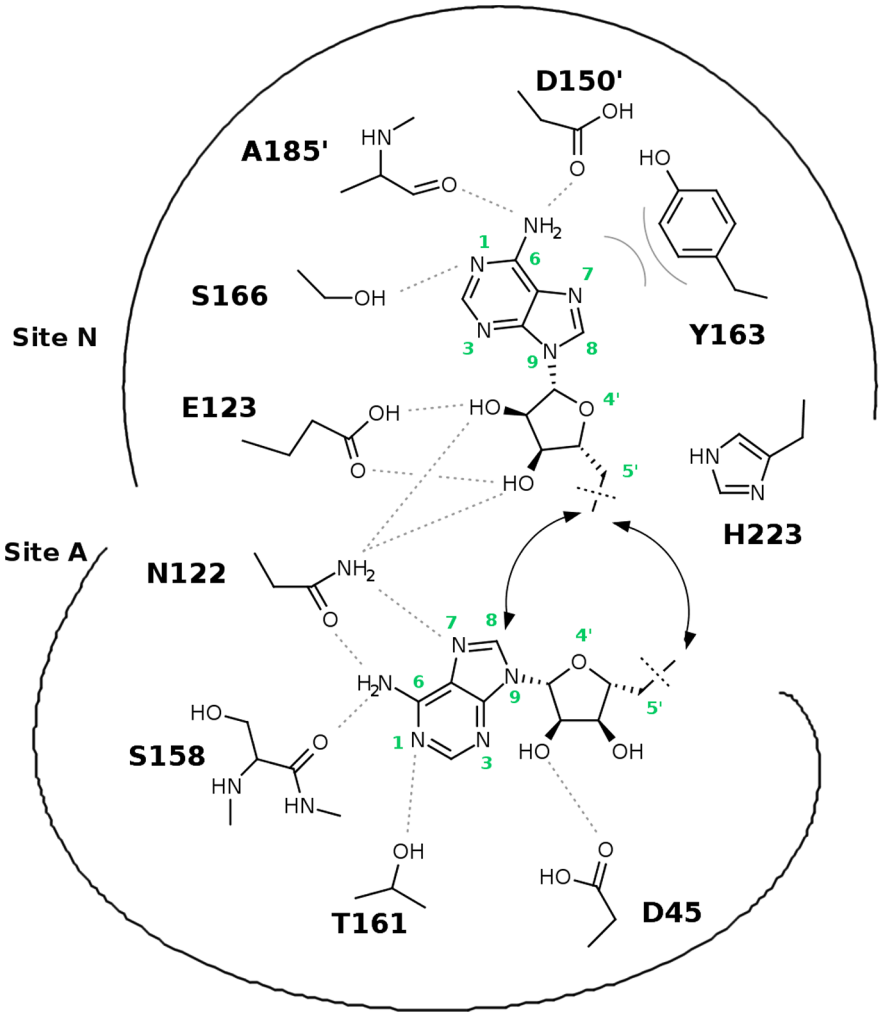

compound	Link between adenosines in site A and in site N	Affinity/ *Lm*NADK (μM)
AppA	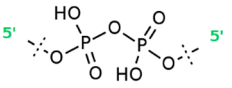	~ 1,000
DTA	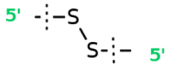	20
A-TGA-A	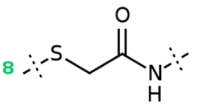	25

Figure 1. Mapping the binding site to design a library: schematic structure of *Lm*NADK1 binding site with known diadenosine inhibitors. Adenosine moieties are linked by a pyrophosphate group (AppA), a disulfide bridge (DTA),[13] or a C8−N5′ thioglycolic acid (A-TGA-A).[15] Corresponding affinities for *Lm*NADK are shown in the table in the right corner.

accurate geometric information. Indeed, FBDD relies on several techniques to evaluate binding, either by affinity measurement (high-concentration assay, microcalorimetry), by structural analysis (X-ray crystallography), or by NMR, which can provide affinity measurement and low resolution structural information but at the expense of large material quantities. Only X-ray diffraction can routinely provide the atomic resolution required to guide precise fragment linking. We imagined using the binary information (binding/not binding) from X-ray crystallography to derive an approximation of ligand affinity. This involves screening, at a given concentration slightly above the expected affinity, chemical compounds that are closely related to each other (and possibly to the first hits). They are more likely to bind and also to share important properties such as solubility to limit potential artifacts. The chemical modifications of a starting fragment with small substitutions or atomic variations are often easier than fragment linking itself, and only a very small amount is necessary for screening by X-ray crystallography. Thus, binding events can precisely pinpoint small differences that are favorable and allow binding site mapping. Optimal substituents should be easily identified, among which some may nicely overlay with atoms from the second fragment or one of its own derivatives. This overlay would provide efficient connectors between these two fragments.

Here, we used a deconstruction approach to synthesize chemical compounds inhibiting bacterial NADK, a novel therapeutic target. Its substrate, NAD, shows an affinity in the millimolar range; hence, an inhibitor in low micromolar range should be sufficient to dramatically impact its enzymatic activity. Interestingly, NAD can be mimicked by a symmetrical diadenosine diphosphate[15] (AppA, Figure 1). In addition, single adenosines were previously shown to share low affinity,[16,17] in the low millimolar range, while occupying the two subpockets of the active site, named A and N for adenine and nicotinamide (Figure 1).

We also showed that the ribose in the subsite A has limited interactions with the protein except for one hydrogen bond. Accordingly, we screened adenine derivatives, instead of adenosines, in order to find new connectors between the two subsites. This led us to design a new 3-atom linker that efficiently connects two adenosines, yielding a compound with low micromolar inhibition of Gram-positive bacterial NADK. Importantly, we identified this compound, hereafter NKI1, as an inhibitor of *S. aureus* infection.

https://dx.doi.org/10.1021/acsinfecdis.9b00368
ACS Infect. Dis. XXXX, XXX, XXX−XXX

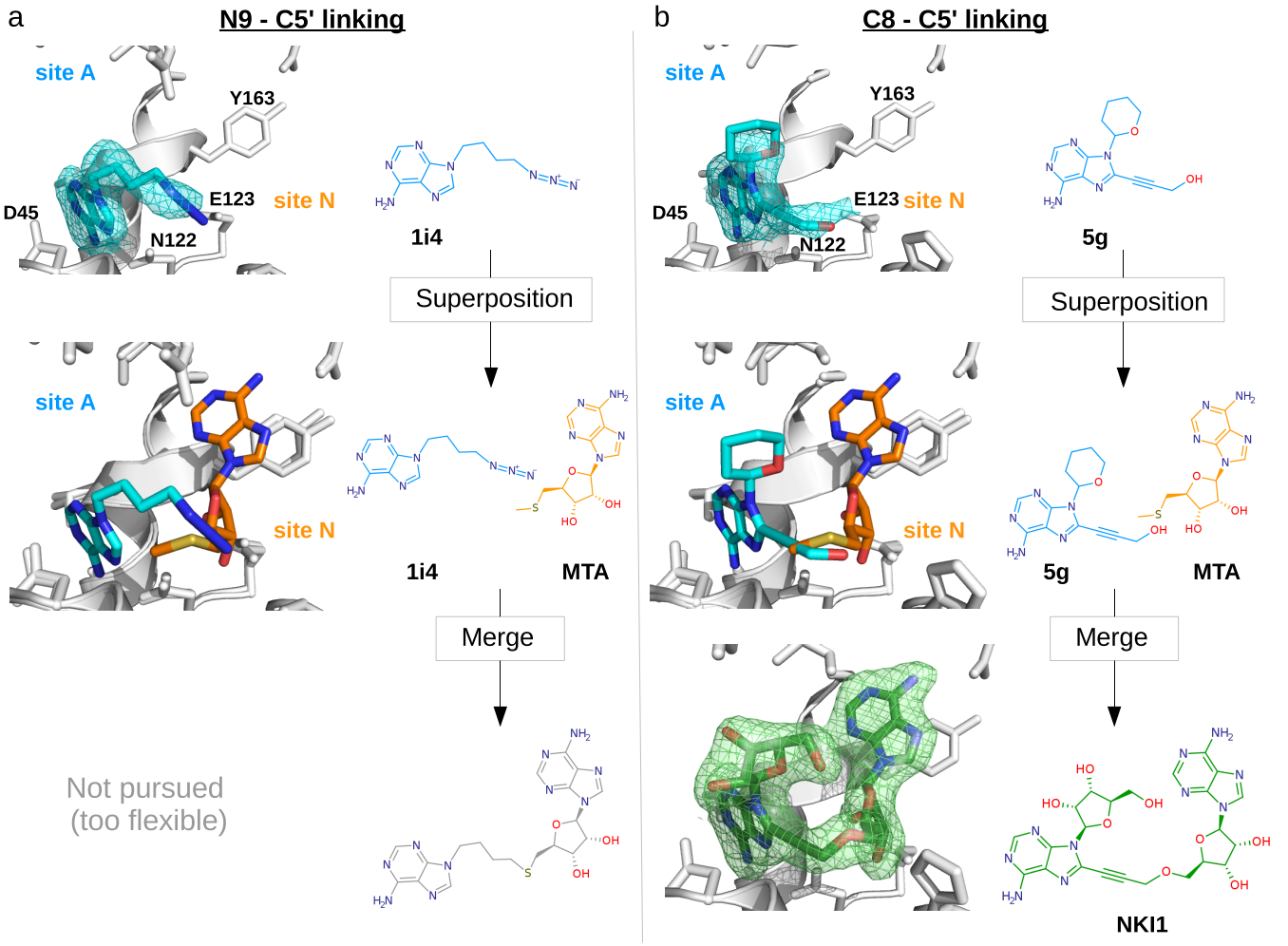

Figure 2. *In crystallo* screening and fragment linking strategy. Two fragment hits bound into the subsite A were used to guide two ways for their linking with an adenosine potentially occupying the subsite N. Linking through position N9 and C5′ or through positions C8 and C5′ is described in panel (a) and (b), respectively. Crystal structures of two N9 and C8 adenine derivatives (**1i4** and **5g**, respectively) bound to *Lm*NADK1 active site are shown in blue. After superimpositions with crystal structures of *Lm*NADK1 bound to **MTA** are also shown (MTA in orange). Finally, the crystal structure of our lead compound **NKI1** bound to *Lm*NADK1 active site. Views of the $2F_o-F_c$ electron density map in the active site with the ligand molecule omitted in the Fourier synthesis. Map is contoured at 1.0 σ. The picture was generated by the program PYMOL (http://pymol.sourceforge.net).

RESULTS

Focused Library Design. We designed a focused library to map the NAD binding site with X-ray crystallography. A former screening campaign demonstrated that various adenosines bearing 5′ substitutions can bind into the active site of the *Listeria monocytogenes* NADK1 (*Lm*NADK1) which is used as a representative enzyme from Gram-positive bacteria.[15−17] This screening allowed the exploration of the binding site in the vicinity of the adenosine 5′ ends, which point toward each other over short distances, as evidenced previously by the 5′-5′ disulfide bridge formed in DTA[15] (Figure 1). It also indicated the rather short N9−N9 or O4′−O4′ distances (6.5 and 5.0 Å, respectively) and an even shorter one between the C8 position of the adenosine in subsite A and the 5′-end of the second adenosine in subsite N. Indeed, the 5′ substituent from subsite N points its thiomethyl group toward the C8 position of the facing adenine at a short distance (S5′−C8:4.1 Å). Importantly, these features are specific for NADKs as the vast majority of NAD(P) binding proteins recognize an elongated conformation of their cofactor.[8]

We wondered whether fragments based on the adenine scaffold could fit and provide a better starting point for drug design or precise tools to map this active site. Furthermore, we considered adenine as an attractive starting point since it can be directly derived from functional annotation for ATP- or NAD-binding proteins or any other adenine/adenosine derivative binding protein. Using a common substructure, here the adenine, allows quicker and clearer comparisons of the impact of various substituents on binding and easier generalization to other targets.

The crystal structure of the wild-type enzyme bound to its substrate or its product highlighted numerous tight contacts with the N1, N6, and N7 of adenine (Figure 1). In contrast, the N3, C8, and N9 were rather solvent-exposed in both subsites. Therefore, positions N3, N9, and C8 could be used to build a new link. Since the N3 position was less amenable to derivatization, we designed a small focused library of adenine bearing substituents at N9 and/or C8 positions.

Screening N9-Derivatives of Adenine by Cocrystallization with *Lm*NADK1. The first adenine derivatives of our focused library included modifications at the N9 position with

https://dx.doi.org/10.1021/acsinfecdis.9b00368
ACS Infect. Dis. XXXX, XXX, XXX−XXX

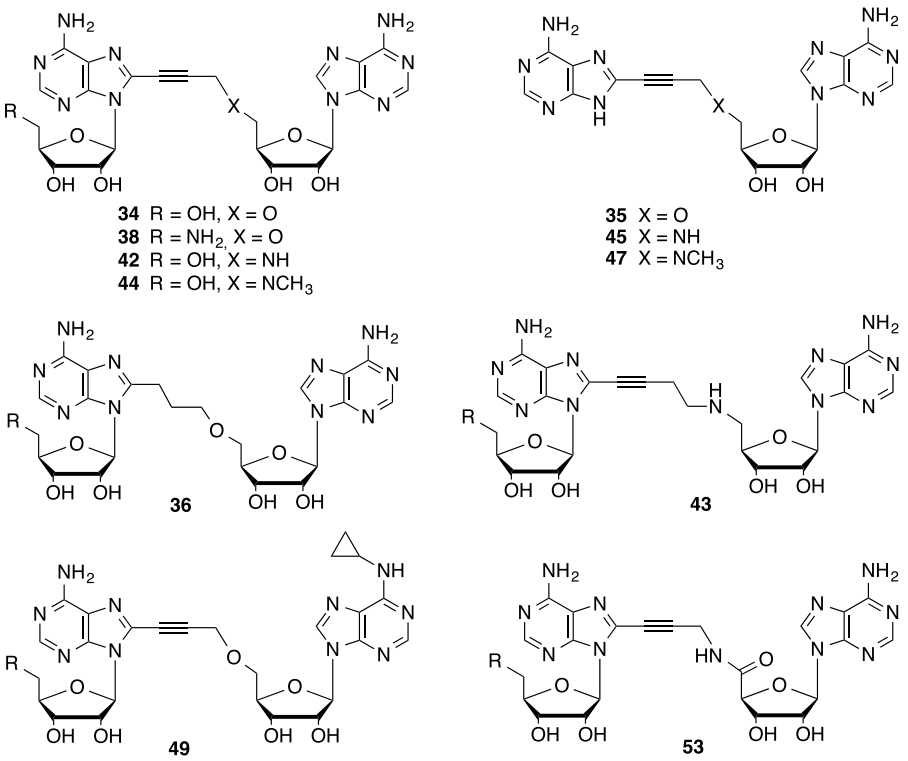

Figure 3. Chemical structures of diadenosine derivatives used in this study.

various short and linear alkyl chains bearing 1, 2, 3, or 4 carbons. They were prepared following classical synthetic routes (Scheme S1). The screening by X-ray crystallography of 20 N9-alkylated adenines (Figure S1) at a final concentration of 10 mM led to only four complexes with *Lm*NADK1 (Figure S2). Most soaking and/or cocrystallization led to an empty crystal structure, suggesting low affinities (>10 mM). No density was observed for any of the small N9-alkyl chains irrespective of the terminal group, either polar, e.g., hydroxyl, thioacetyl, amino, azido, or hydrophobic, e.g., alkynyl (Figure S1). This suggests that these small substituents fail to provide favorable interactions in the A or N subsite. Four N9-derivatives (Figure S2) could be detected in our screen, and they generally harbored a 4-carbon-long chain, as did the 9-(4-azidobutyl)-adenine (compound **1i4**, Figure S2a). However, these N9 substitutions were relatively mobile, again with little or no favorable interaction with the protein. Nevertheless the 4-azidobutyl extension of compound **1i4** superimposed quite well with the 5′ end of an adenosine in subsite N (Figure 2a). This path was not pursued further, as the link would be too flexible to yield a high-affinity compound.

The rather limited success of this focused screening of adenines substituted in N9 only led us to re-evaluate the same substitutions on an adenine harboring, in addition, a bromo substituent at the C8 position. The additional bromine atom at the C8 position was selected to improve the hit-rate, since brominated adenosine previously showed a gain in affinity in the adenosine series.[16,17] Bromination was performed straightforwardly, and 10 out of 11 compounds were detected bound into the subsite A (Figure S3), but their pending arms revealed no particular hot-spot for interactions on the path to the N subsite (Figure S4). Because these substituted adenines only occupy the subsite A, they represent a starting point to grow a fragment from subsite A into a larger compound occupying the whole active site. On the contrary, the subsite N remained empty for all the adenines tested. The tilted side chain of tyrosine Y163 may limit nucleobase entrance in this subsite, a hindrance counterbalanced by the presence of a ribose moiety in adenosine derivatives. Accordingly, a compound made of two adenines linked by their respective N9 position would not be optimal. Thus, the privileged fragment for subsite N remained adenosine.[15−17] However, the first round of screening highlighted no valuable path from the N9 position of an adenine placed in the subsite A toward a facing 5′-end from an adenosine placed in the subsite N. In order to find a more suitable link toward the subsite N, we turned to characterize substituted adenines at position C8 that would be compatible with binding into the subsite A.

Screening C8-Derivatives of Adenine by Cocrystallization with *Lm*NADK1. Previously, *in situ* bond formation between two bound adenosines revealed a short C8−C5′ linker, a thioacetamide moiety, able to connect subsites A and N (A-TGA-A, Figure 1). This link provided the first NADK inhibitor active on bacterial culture *in vitro*.[16] Thus, we considered other substitutions at the C8 position of adenine with the aim of linking an adenine in the subsite A and an adenosine in subsite N. This substitution could fit in the narrow and rather hydrophobic groove formed by Leu49 and Gly46.

First, position C8 of adenine was substituted with small alkyl groups (Figure S5). The key synthetic step involved a ring closure reaction of 2,4,6-triaminopyrimidine (Scheme S2). Methyl and ethynyl groups (compounds **14a−d** and **3b**) were accommodated nicely (Figure S6). On the contrary, a hydrophobic but flexible ethyl group disfavored binding (compound **10**, Figure S7). Six other small and flexible substituents at the C8 position did not show any binding (Figure S7).

https://dx.doi.org/10.1021/acsinfecdis.9b00368
ACS Infect. Dis. XXXX, XXX, XXX−XXX

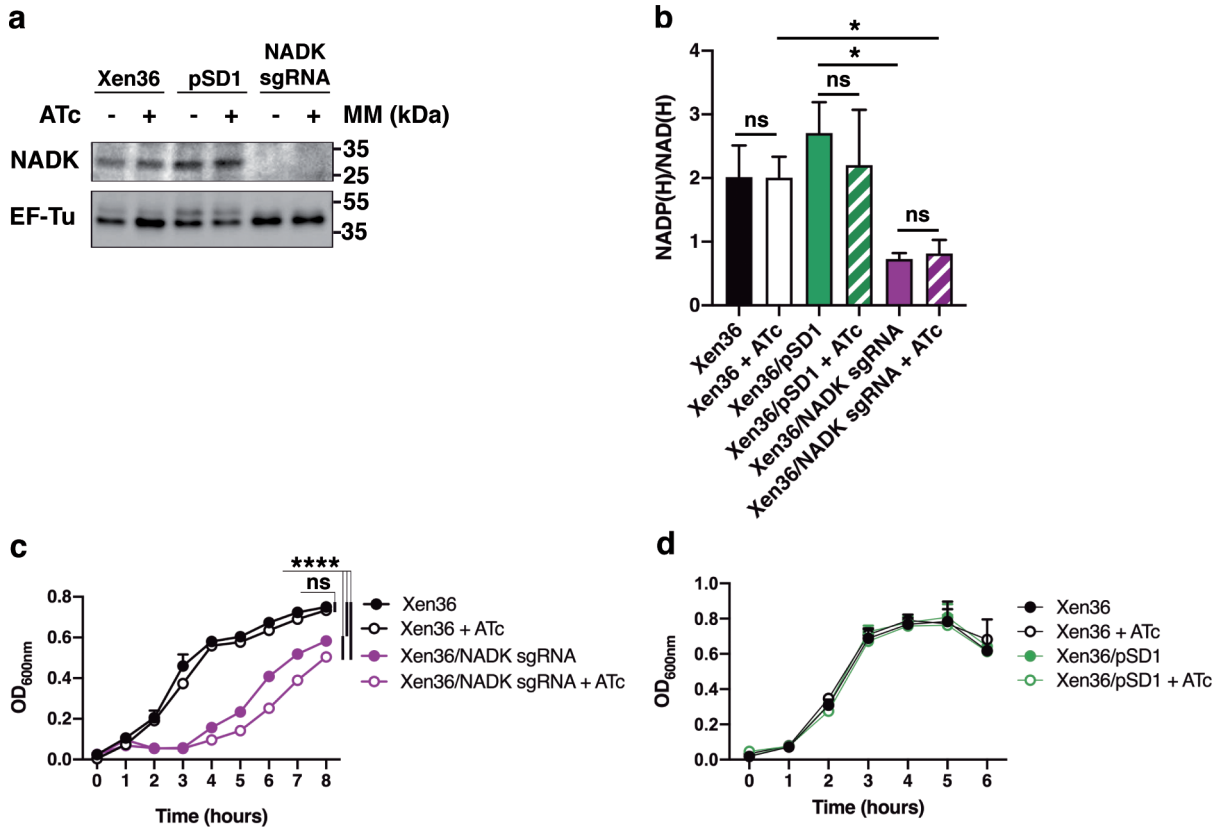

Figure 4. NADK is important for *S. aureus* growth. Bacterial growth was monitored at OD_{600nm} in BHI broth at 37 °C with and without ATc induction. (a) Total bacterial lysates of wild-type (Xen36), control (pSD1), and *ppnK* knock-down (NADK sgRNA) strains were analyzed by immunoblotting using anti-NADK and anti-EF-Tu antibodies. EF-Tu is used as a loading control. The data shown are representative of independent data from two experiments. (b) Levels of NAD(H) and NADP(H) and their ratio were determined by using the NAD/NADH-Glo and NADP/NADPH-Glo assays after growing wild-type (Xen36), control (Xen36/pSD1) and *ppnK* knock-down (Xen36/NADK sgRNA) strains for 6 h (n = 3). Bars indicate the standard errors of the means of biological replicates. Comparison of data was performed using a t test (ns: nonsignificant, *p < 0.05). (c) Growth curves of wild-type (Xen36) and *ppnK* knock-down (Xen36/NADK sgRNA) strains (n = 6). Bars indicate the standard errors of the means of biological replicates. Comparison of data was performed using two-way analysis of variance (ns: nonsignificant, ****p < 0.0001). (d) Growth curves of wild-type (Xen36) and control (Xen36/pSD1) strains (n = 6). Bars indicate the standard errors of the means of biological replicates. Comparison of data was performed using two-way analysis of variance.

Then, a 3-hydroxypropynyl group, named hereafter propargyl alcohol, was introduced at position C8 via a Sonogashira coupling reaction (Figure S8). This substitution led to a clear electron density in the crystal structure only in the presence of a cyclic substituent at the N9 position (compound **5g**, Figure S9). This behavior was similar to that in the absence of substituents in position C8 (compound **1g**). Accordingly, the propargyl moiety could be accommodated, but its polar and flexible end might partially counterbalance its hydrophobic interactions with the neighboring Leu49. Nevertheless, this structure showed that the triple bond of the propargyl group in position C8 fits perfectly into a narrow hydrophobic groove that is conserved among all known NAD kinases.

Interestingly, the hydroxyl end group of the propargyl alcohol superimposed well with the position of the sulfur atom of a methylthioadenosine molecule that would bind into the subsite N (MTA, Figure 2b). This rather good match (S5′−O distance: 1.2 Å) suggested a new linker for the connection of the adenine in subsite A to an adenosine in subsite N, with a more rigid and more hydrophobic moiety than the formerly discovered thioglycolate linker.

Propargyl as a New Connector. These results prompted us to evaluate propargyl alcohol as a new linker between the subsites A and N. We synthesized a diadenosine derivative linked by the propargyl moiety (compound **34**, NKI1, Figure 3) as well as an adenine linked by the same connector to an adenosine (compound **35**). Both double-headed molecules were cocrystallized with *Lm*NADK1 and nicely fit into the whole active site. In both cases one adenosine head occupies the subsite N, while the subsite A accommodates either the other adenosine moiety or an adenine moiety (Figure S10).

Subsequently the *O*-propargyl linker was replaced by a *N*-propargyl linker (compound **42**) or a *N*-methylpropargyl linker (compound **44**). These new compounds showed little gain in affinity against *Lm*NADK or against the NADK from *S. aureus*, another clinically relevant Gram-positive pathogen (Figure S10), which shares 57% of sequence identity (corresponding to 40 strictly conserved residues among the 50 ones lying within a distance shorter than 8 Å to NADP) with its listerial counterpart. Noteworthy, the active concentration of these novel compounds is 3 orders of magnitude lower than the millimolar affinity of NAD for these kinases, which suggested a potential therapeutic window for treatment as an antibiotic. Their solubility was not improved and their selectivity index toward the human counterpart was not significantly impacted.

Interestingly, in the presence of a ribose in the subsite A, most crystal structures revealed two hydrogen bonds involving its 5′ hydroxyl group with the oxygen/nitrogen of the

https://dx.doi.org/10.1021/acsinfecdis.9b00368
ACS Infect. Dis. XXXX, XXX, XXX−XXX

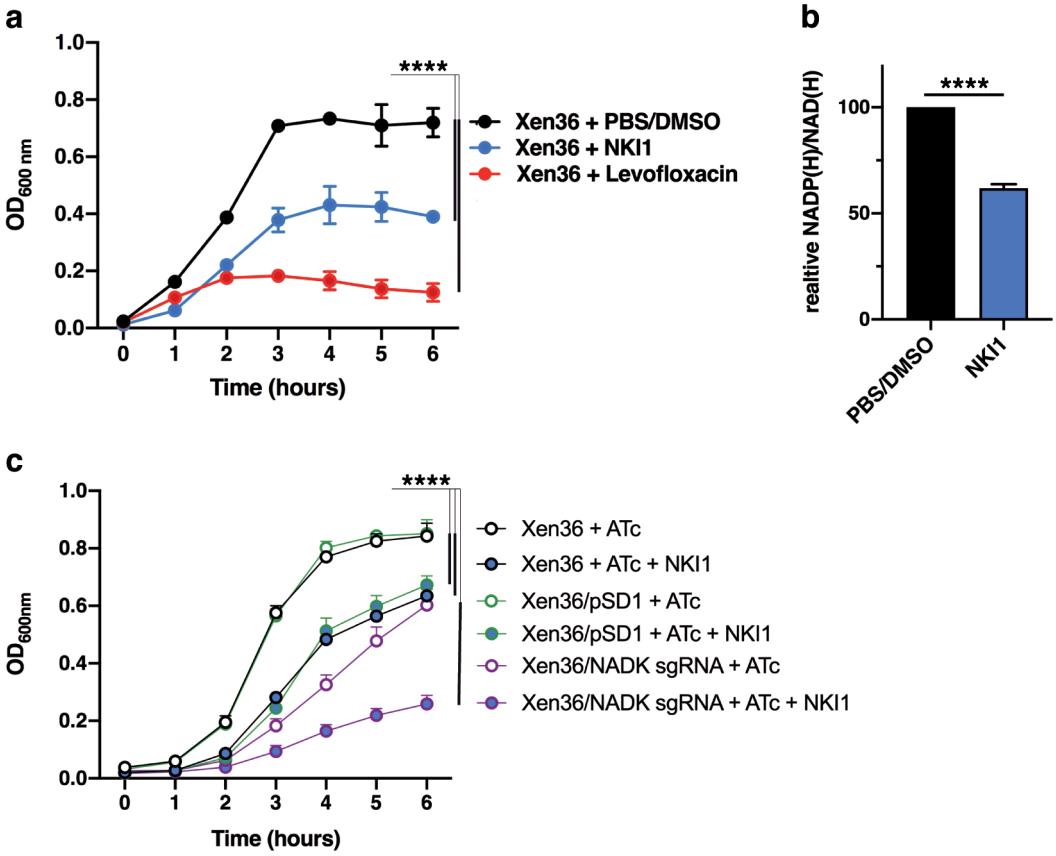

Figure 5. NKI1 inhibits *S. aureus* growth *in vitro*. (a) Growth of *S. aureus* Xen36 was monitored at OD_{600nm} in BHI broth at 37 °C. BHI broth was supplemented with PBS/10% DMSO, 0.01 μg/mL NKI1 or 10 μg/mL levofloxacin (n = 6). Bars indicate the standard errors of the means of biological replicates. Comparison of data was performed using two-way analysis of variance (****p < 0.0001). (b) Levels of NAD(H) and NADP(H) and their ratio were determined by using the NAD/NADH-Glo and NADP/NADPH-Glo assays after growing the wild-type Xen36 strain for 6 h in BHI with or without 0.01 μg/mL NKI1 (n = 3). Bars indicate the standard errors of the means of biological replicates. Comparison of data was performed using a t test (****p < 0.0001). (c) Growth curves of wild-type (Xen36), control (Xen36/pSD1), and *ppnK* knock-down (Xen36/NADK sgRNA) strains in BHI broth supplemented with ATc, with and without 0.01 μg/mL NKI1 (n = 6). Bars indicate the standard errors of the means of biological replicates. Comparison of data was performed using two-way analysis of variance (****p < 0.0001).

propargyl or the nearby O4′ oxygen from the ribose moiety in the subsite N (Figure S10). These internal interactions can stabilize the bound conformation. An attempt to reinforce these interactions with a hydrogen-bond donor failed, as the corresponding 5′-amino group points toward the catalytic aspartate due to a rotation of the ribose (compound **38**, Figure S10).

The inhibitory potency of the diadenosine derivatives was tested on recombinant NADKs from *L. monocytogenes* and *S. aureus*. IC_{50} were determined by measuring formation of reduced NADP produced by the glucose-6-phosphate dehydrogenase coupling enzyme as a readout of NADK activity.[15−17] Inhibition in the low micromolar range was observed for diadenosine derivatives linked by a *O*- or *N*-(methyl)-propargyl group (compounds **34**, **42**, **44**), while derivatives bearing a flexible three-carbon spacer (*O*-propyl linker, compound **36**), an amide group (compound **53**) or a four-carbon spacer (compound **43**) showed little or no activity against both enzymes (Figure S10).

NADK Is Critical for Growth of *S. aureus*. We next addressed the importance of NADK on *S. aureus* growth *in vitro*. We investigated the impact of decreasing expression of the NADK gene *ppnK* on the growth of *S. aureus* Xen36, a clinical strain. We used the CRISPR interference-based approach described by Zhao and colleagues[18] to knock-down *ppnK*. The Xen36 strain was transformed with the *E. coli*/*S. aureus* shuttle plasmid pSD1 or pSD1 containing a single guide RNA (sgRNA) complementary to *ppnK*-specific sequence and the catalytically dead Cas9 (dCas9). Expression of the sgRNA and dCas9 was under the control of the constitutive *S. aureus* promoter P_{lgB} and the anhydro-tetracyclin (ATc) inducible promoter P_{tetO}, respectively. Production of NADK by the wild-type, control, and knock-down strains was assessed by immunoblotting. As expected, levels of NADK were strongly reduced in the knock-down strain compared to that of the wild-type and control strains (Figure 4a, Figure S11b). Decreased expression of *ppnK* in the knock-down strain in absence of ATc was presumably due to the known basal activity of the P_{tetO} promoter. We next determined the NADP(H)/NAD(H) ratio in the wild-type, control, and knock-down strains (Figure 4b). The ratio was significantly lower in the knock-down strain than in the wild-type (p = 0.03) and control (p = 0.01) strains, confirming that the sgRNA targeted *ppnK*. Decreased NADP(H)/NAD(H) ratio in the knock-down strain in absence of ATc corroborated basal activity of the P_{tetO} promoter. Having demonstrated the efficiency of the NADK knock-down, we then measured growth of the wild-type, control, and knock-down strains at OD_{600nm} in BHI with or without ATc. Xen36/NADK sgRNA strain had multiple growth defects in BHI including increased

https://dx.doi.org/10.1021/acsinfecdis.9b00368
ACS Infect. Dis. XXXX, XXX, XXX−XXX

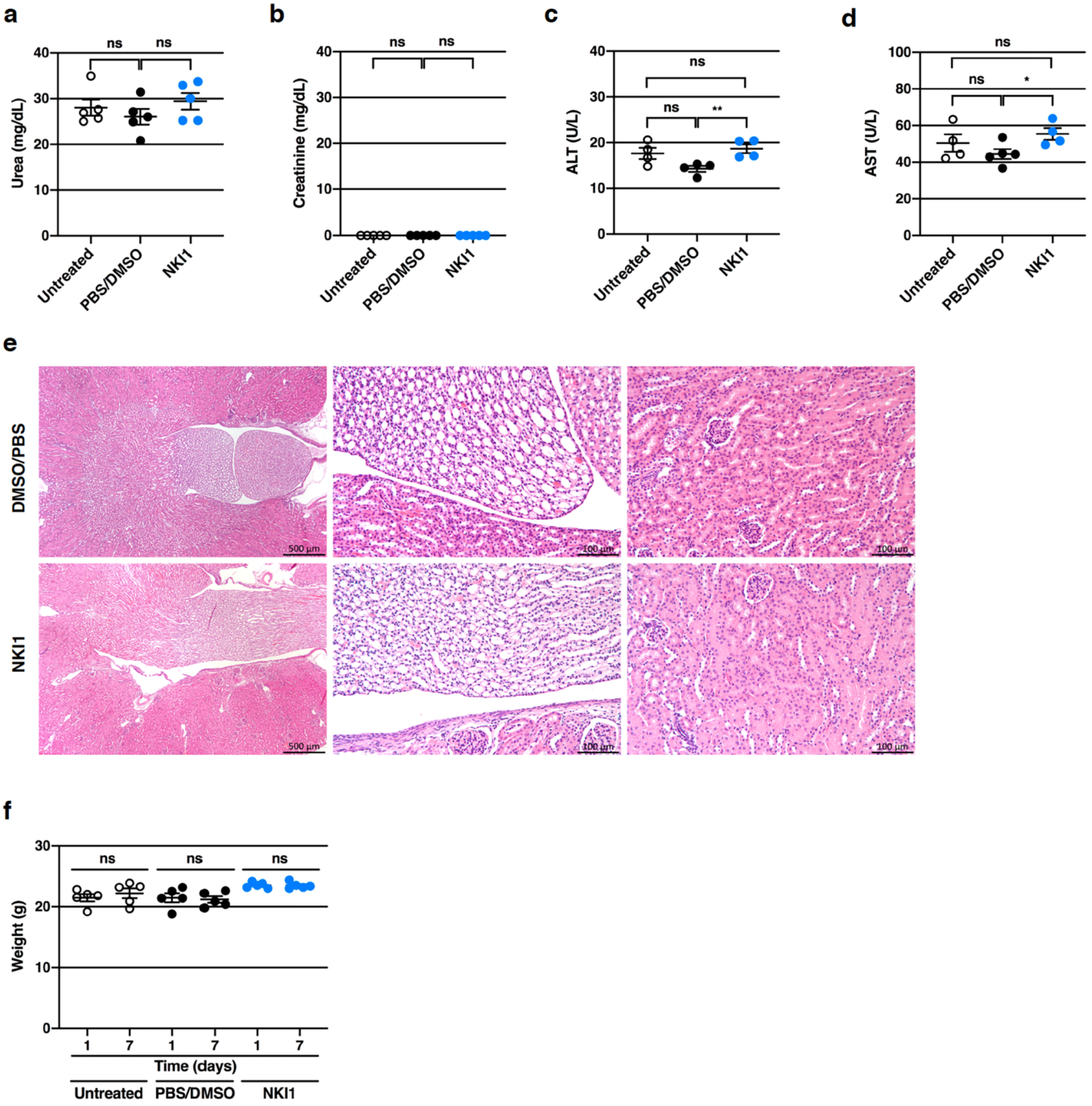

Figure 6. NKI1 is not toxic to mice. BALB/c mice were left untreated or treated daily intraperitoneally with PBS/10% DMSO or 2 mg NKI1. (a–d) Blood was collected 7 days postinoculation for quantitation of urea (a), creatinine (b), alanine aminotransferase (c), and aspartate aminotransferase (d) using Reflotron strips. Data are means ± SEM. (e) Histopathological analyses of kidneys of mice 7 days post-treatment. (f) Weight of mice at day 1 and day 7 post-treatment. Data represent mean weights ± SEM. Comparison of data was performed using a *t* test (ns: nonsignificant, $*p < 0.05$, $**p < 0.01$).

lag time, decreased doubling time and reduced density in stationary phase compared to the wild-type strain (Figure 4c). These defects were even more pronounced when Xen36/NADK sgRNA was grown in BHI/ATc, while ATc had no effect on growth of the wild-type strain (Figure 4c and Figure S11a). Growth defects in the absence of induction substantiated expression of dCas9 mediated by basal P_{tetO} activity. In contrast to growth of the knock-down strain, growth of the pSD1 control strain was similar to that of the wild-type strain (Figure 4d). Altogether, these results highlight the capital role of *ppnK* for *S. aureus* growth.

Given that NADK was critical for *S. aureus* growth, we next examined whether diadenosine derivatives could inhibit bacterial multiplication *in vitro*. The addition to *S. aureus* cultures of a diadenosine linked by a propargyl (compound **34**, hereafter NKI1), strongly affected bacterial growth (Figure 5a). The lag, log, and plateau phases of NKI1 treated bacteria were significantly impaired compared to that of bacteria treated with the solvent. As expected, growth of bacteria treated with

https://dx.doi.org/10.1021/acsinfecdis.9b00368
ACS Infect. Dis. XXXX, XXX, XXX−XXX

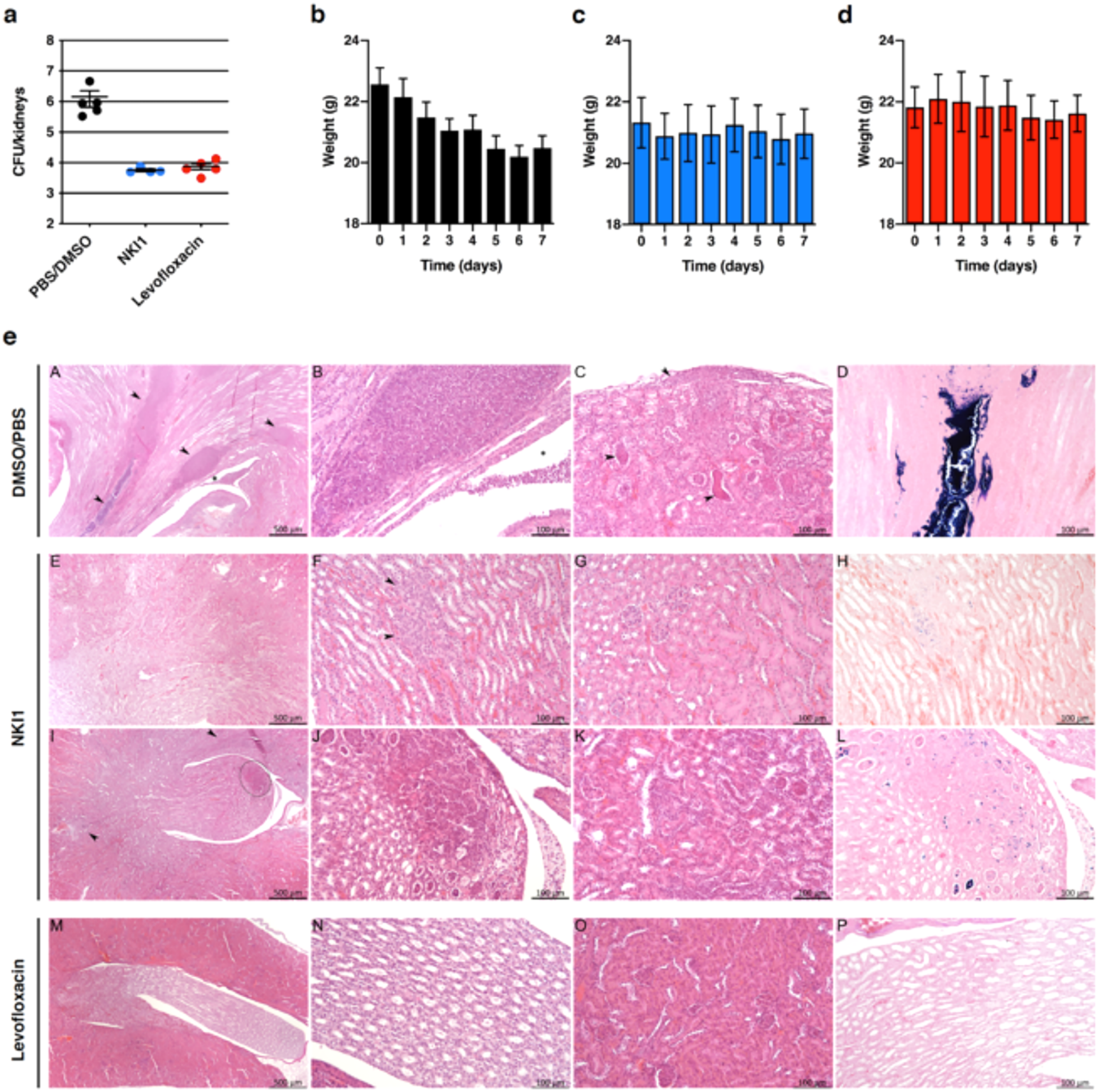

Figure 7. NKI1 treatment controls *S. aureus* infection *in vivo*. BALB/c mice were infected intravenously with 5×10^7 *S. aureus* Xen36 and treated daily intraperitoneally with 2 mg NKI1 or 2 mg levofloxacin. Control mice received PBS/10% DMSO. (a) Bacterial burden in kidneys of mice 7 days postinfection. Data are mean CFUs in two kidneys ± SEM. (b–d) Daily weight of infected mice of the control group (b), NKI1 group (c), and levofloxacin group (d). The bars represent mean weights ± SEM. (e) Histopathological analyses of kidneys of mice 7 days postinfection. Representative images of hematoxylin/eosin and/or Gram stained sections from untreated (n = 8) or treated mice (n = 8). Panels A–D, murine pyelonephritis of the control group (DMSO/PBS). Panel A, ascending inflammation reaching the cortex and necrosis of the papilla. Arrowheads, suppuration. Panel B, infiltration of neutrophils in the renal tubes and interstitium. Panel C, infiltration of neutrophils in the cortex and subcapsular space. Arrowheads, infiltration in the renal tubes. Panel D, Gram-stained bacteria. Panels E–L, lesions of NKI1-treated mice. Panels E–G, small cortical inflammatory infiltrates. Arrowheads, inflammatory infiltrates. Panel H, Gram-strained bacteria. Panels I–K, mild pyelonephritis, Panel L, Gram-stained bacteria. Panels M–P, kidney sections of mice treated with levofloxacin. Panels M–O, absence of lesions. Panel P, absence of bacteria.

levofloxacin was severely reduced compared to growth of bacteria in absence of antibiotics. We next determined the NADP(H)/NAD(H) ratio in bacteria grown in BHI with or without NKI1 (Figure 5b). The ratio was significantly lower in bacteria treated with NKI1, suggesting that NKI1 targeted NADK. To determine if NKI1 antibacterial activity was solely dependent on NADK inhibition, we then measured growth of the wild-type, control, and knock-down strains at OD_{600nm} in BHI with ATc, with and without NKI1. Growth of the three strains were significantly impaired by addition of NKI1,

https://dx.doi.org/10.1021/acsinfecdis.9b00368
ACS Infect. Dis. XXXX, XXX, XXX–XXX

confirming the antibacterial activity of NKI1 and suggesting that other pathways may be affected by NKI1 when its primary target is depleted (Figure 5c). Together, these results indicate that NKI1 inhibits growth of *S. aureus* by targeting NADK and presumably other mechanisms.

NKI1 Is Not Toxic to Human Cells *In Vitro* or to Mice *In Vivo*. Because mammals also possess NADKs, we determined the effect of NADK inhibitors on human cell lines. All synthesized diadenosine derivatives, including NKI1, were assayed for cytotoxicity on MRC-5 human fetal lung fibroblasts. The percentage of dead cells after 3 days of incubation with NKI1 was 0 ± 4% at a concentration of 10^{-5} M and 0 ± 6% at 10^{-4} M. Therefore, NKI1 acts as an antibiotic without detrimental effects on human cells. Before testing NKI1 toxicity *in vivo*, we assessed the stability of NKI1 by standard liver microsomal and plasma stability assays *in vitro*. We could not detect any significant degradation of NKI1 for 1 h at 37 °C in the presence of liver drug metabolizing enzymes (Figure S12a) or plasma hydrolytic enzymes (Figure S12b), pointing to high stability of the compound.

To determine the impact of the compound on organ functions, we next analyzed markers of organ failure in plasma from untreated BALB/c mice or from mice treated with NKI1 or PBS/DMSO used as the vehicle for NKI1. We found that urea, creatinine, alanine transaminase and aspartate transaminase were not increased in mouse plasma upon NKI1 treatment nor upon injection of the vehicle alone, consistent with preserved kidney, liver, muscle, and heart functions (Figure 6a−d). Histological analysis confirmed the absence of detectable kidney abnormalities in mice treated with NKI1 (Figure 6e). Additionally, treated mice did not show any physical signs of discomfort and did not lose any weight (Figure 6f).

NKI1 Contributes to Bacterial Clearance in *S. aureus* Infected Mice. Given that NKI1 has an antibacterial activity against *S. aureus in vitro*, the effect of NKI1 was addressed *in vivo*. We evaluated the antibacterial activity of the compound in a murine model of acute hematogenous pyelonephritis induced by the *S. aureus* Xen36 strain. BALB/c mice were infected intravenously with 5×10^7 bacteria and received daily intraperitoneal injections of 100 mg/kg NKI1 or levofloxacin as a control antibiotic for 7 days. A vehicle control group received PBS/DMSO. In the absence of antibiotic treatment, high levels of *S. aureus* were detected in the kidneys 7 days postinfection (Figure 7a). In contrast, daily treatment with NKI1 led to an important decline in the kidney bacterial burden. Levofloxacin treatment led to a similar decrease in bacterial counts. Untreated mice progressively lost weight with time (Figure 7b), while the weight of mice treated with NKI1 or levofloxacin remained stable (Figure 7c,d), confirming the efficacy of both antibacterial compounds.

We next performed a histologic examination of kidneys removed 7 days postinfection with the *S. aureus* Xen36. The microscopic comparison of kidney sections is shown in Figure 7e. Kidneys from untreated mice exhibited marked pyelonephritis with papillary necrosis and infiltration of neutrophils (panel A), extending in the renal tubes and interstitium from the papilla to the cortex (panels A and B) and even to the subcapsular space (panel C). High bacterial loads were detected in kidney lesions (panel D). In contrast, kidneys of mice treated with NKI1 had no lesion or a few small abscesses or inflammatory infiltrates in the cortex (panels E−G) with minimal amount of bacteria (panel H). Pyelonephritis detected in a few mice was less severe than that observed in untreated mice (panels I−K) with much lower bacterial loads (panel L). Besides occasional inflammatory infiltrates in the cortex (data not shown), kidneys of mice treated with levofloxacin did not display any lesion (panels M−O) or bacteria (panel P).

As the difficulty of treating antibiotic resistant infections is a growing concern, we next investigated whether NKI1 could be active on the MRSA strain Xen31 *in vitro* and in the murine model of hematogenous pyelonephritis described above. Growth of Xen31 *in vitro* was strongly affected by NKI1, although not to the level obtained upon levofloxacin treatment, which was near total inhibition of growth (Figure S13a). Efficacies of NKI1 and levofloxacin were then compared *in vivo* by determining the decrease in the number of bacteria in kidneys of infected mice. Levofloxacin and NKI1 at 100 mg/kg daily resulted in decreases of 1.5 and 0.5 $\log_{10}$ CFU/kidney from control levels, respectively (Figure S13b). Mice treated with NKI1 or levofloxacin lost weight with time (Figure S13d, S13e), albeit not to the levels exhibited by untreated mice (Figure S13c), confirming efficacy of both compounds. The histologic assessment was in agreement with the weight and bacterial burden quantification, demonstrating that NKI1 and levofloxacin were capable of reducing the severity of lesions in mice infected with the MRSA strain Xen31 (Figure S13f). Untreated mice displayed pyelonephritis characterized by necrosis of the papilla and infiltration of neutrophils at the periphery of necrotic foci, in the cortex and in the pelvic cavity (Figure 7, panels A−C). Massive amounts of bacteria were detected in the papillary necrotic area (Figure 7, panel D). In contrast, pyelonephritis was not detected in mice treated with NKI1. Kidneys were either free from lesion and bacteria (Figure 7, panels E−H) or displayed focal abscesses and bacteria in the cortex (Figure 7, panels I, K, and L) without any lesion in the papilla (Figure 7, panel J). After levofloxacin treatment, some mice did not display any lesion or bacteria in the kidneys (Figure 7, panels M−P), while others exhibited pyelonephritis (Figure 7, panels Q−T). However, neutrophil infiltration and bacterial load were reduced compared to those observed in untreated mice. Taken together, these results suggest that antibacterial activity of NKI1 is not restricted to MSSA but extends to drug resistant strains.

DISCUSSION

Discovery and design of new antibacterial compounds is gaining renewed interest due to the emergence of new threats from drug-resistant bacteria. NADKs represent attractive drug targets that have so far been understudied. We hypothesized that adenine could provide a privileged scaffold onto which substitution could rapidly answer the question regarding hot-spots in the region linking the two subsites. Knowledge of *a priori* binders such as the natural ligands and their fragments or isosteric analogues may represent alternative entities suitable to interrogate the possible output of a given screening approach. Previously, two derivatives of adenosine were linked *in situ*[16] but the resulting compound was suboptimal, showing activity in the 25−50 μM range, similar to the natural reaction product, NADP.

In this study, we screened a focused library of adenine derivatives to identify a new linker. It led to a potent chemical compound, the best inhibitor described so far for a NADK, and the first which is active *in vivo*. We targeted *S. aureus* as it is among the most prominent opportunistic pathogenic bacteria. It belongs to the worrisome ESKAPE group of bacteria

https://dx.doi.org/10.1021/acsinfecdis.9b00368
ACS Infect. Dis. XXXX, XXX, XXX−XXX

(*Enterococcus faecium*, *Staphylococcus aureus*, *Klebsiella pneumoniae*, *Acinetobacter baumannii*, *Pseudomonas aeruginosa*, *Enterobacter* sp.) with a high potential to become antibiotic resistant and difficult to treat. While NADK had been convincingly demonstrated to be essential for the survival of several bacteria including *Escherichia coli*,[4] *Bacillus subtilis*,[5] and *Mycobacterium tuberculosis*,[6] it was not clear whether the NADK gene *ppnK* was important for *S. aureus* growth as apparently conflicting results had been published.[19−23] Our data indicated that the knock-down of NADK has a strongly deleterious effect on *S. aureus* growth, consistent with the importance of the enzyme reported by Bae et al.,[21] Chaudhuri et al.,[22] and Yamachika et al.[23] *S. aureus* has the remarkable capacity to trigger a wide array of infections in susceptible hosts, ranging from skin, soft tissue, bone, joint, kidney, and lung infections to life-threatening bacteremia, endocarditis, sepsis, and toxic shock syndrome.[24] Several animal models mimicking human infections have been developed to study *S. aureus* pathogenicity and test drug candidates,[25−28] including the murine model of hematogenous pyelonephritis.[29,30] We show for the first time that the bactericidal potential of NKI1 translates *in vivo* into containment of *S. aureus* induced pyelonephritis, which presumably involves host defense mechanisms. NKI1 activity was similar to that of levofloxacin, a member of the fluoroquinolone family of antibiotics guideline-recommended to treat acute pyelonephritis in humans[31,32] and shown to control pyelonephritis induced by *S. aureus* intravenous inoculation in mice.[30] Both compounds were efficient at controlling bacterial multiplication in kidneys. As a result, the number and size of tissular lesions and cellular damages were reduced or abrogated. Treated mice recovered from the infection as shown by the absence of physical signs of disease and weight loss. Interestingly, NKI1 was also active on Xen31, an MRSA strain. While NKI1 activity was similar on Xen31 and Xen36 *in vitro*, *in vivo* activity against Xen36 was superior to that against Xen31. Xen36 is derived from the Wright strain isolated from a bacteremic patient (ATCC49525). Xen31 was isolated independently from a patient hospitalized in New York City.[33] Xen31 and Xen36 are thus two clinical isolates that presumably differ in many ways including their sensitivity to methicillin and possibly virulence. These characteristics could account for the different levels of efficacy seen with NKI1 but also with levofloxacin.

This example illustrates the potential of biology-driven fragment-based drug design where ligand screening is precisely guided by means of X-ray crystallography. Our study exemplified the successful application of a rational linking strategy to derive a new inhibitor. This also illustrates a possibly useful strategy for general FBDD, where each hit to be linked is rapidly derivatized with variable extensions. Despite the absence of precise monitoring of the affinity toward the target, comparisons of closely related compounds can pinpoint either affinity cliffs when small substituents prevent binding or interaction hot-spots when substituting arms show favorable contacts. This can lead to rapid mapping of the active site. The structural information gained so far suggests further possible improvement of the new inhibitor.

■ CONCLUSION

We identified the first bacterial NAD kinase inhibitor, NKI1, active both *in vitro* and *in vivo*. Importantly, NKI1 is active against drug-resistant pathogenic bacteria. On-target activity is currently being investigated in *S. aureus* using proteomic and genetic approaches, based on drug affinity chromatography coupled to mass spectrometry and modulation of gene expression, respectively. The favorable activity against staphylococcal infections and the absence of acute toxicity open the way for further optimization of the lead compound NKI1 against various bacterial pathogens.

■ METHODS

Expression, Purification, and Activity Assay. His-tagged *Lm*NADK1 was expressed and purified on cobalt-based IMAC resins (Clontech) as previously published.[16] A similar procedure was followed for the orthologs from *S. aureus*. The NAD kinase activity was determined by measuring the absorbance at 340 nm to follow the formation of reduced NADP produced by a coupling enzyme (Glucose-6-phosphate dehydrogenase from yeast). This enzyme and its substrate were purchased from Sigma-Aldrich. The assay was performed in a 0.5 mL sample of 50 mM Tris-HCl pH7.4, 10 mM $MgCl_2$, 2 mM sodium citrate, 1 mM glucose-6-phosphate at 30 °C using a spectrophotometer Eppendorf ECOM 6122. Half-inhibitory concentrations (IC_{50}) were determined, in the presence of 1 mM NAD and 4 mM ATP (for *Lm*NADK1) or 2 mM ATP for *S. aureus* NADK. Dixon plots were used to determine K_I in the presence of 4 mM ATP and three NAD concentrations (0.2, 0.5, and 1 mM). We also checked that the inhibitors had no effect on the coupling enzymes activity.

Chemical Synthesis. The synthesis of adenine derivatives used in this study (see Supporting Information, Figure S1) involved the *N*-9 alkylation of a purine derivative (adenine, 6-chloropurine or 8-methyl-adenine), further conversion of the alkyl alcohol into the corresponding thioacetyl, azido, or amino functional groups. Bromination at the C8 position and subsequent Sonogashira cross-coupling reaction afforded the difunctionalized adenine derivatives (compounds **1**−**9**, Scheme S1). The preparation of C8 alkylated adenine derivatives (**9**−**15**, Scheme S2) involved the ring closure of the 4,5,6-triaminopyrimidine in the presence of an acid or amide (classical heating or under MW irradiation), followed by *N*-9 alkylation.

The synthesis of the diadenosine derivatives (Figure 3) involved Sonogashira cross-coupling reaction of the 8-bromoadenosine derivative **30** or **31** (see Supporting Information) with an appropriate alkyne derivative synthesized as illustrated in Scheme S3. Subsequent deprotection afforded the target compounds (**34**, **36**, **38**, **42**, **43**, **44**, **49**, **53**) in good overall yield.

Crystallization. A dedicated crystallization kit (24-conditions) was set up to ensure reproducibility from one protein sample to another. Crystals were grown by mixing 1 μL of the protein solution concentrated at 9 mg/mL and complexed with 5′-deoxy-5′-(methylthio)adenosine (MTA) with an equal volume of crystallization buffer (30 mM sodium bromide, 220 mM potassium citrate, pH 4.8−5.1, glycerol 6%, 15−16% w/v polyethylene glycol 400), equilibrated over 0.5 mL of the same buffer. As described previously, the complexes with bound ligands were solved using crystals in the orthorhombic form. After growing them in the presence of MTA, crystals were soaked with a 10 mM concentration of the desired ligand in a pre-equilibrate hanging-drop.

Crystallographic Studies. X-ray structure determinations were performed using molecular replacement. Refinement was performed using Phenix.[34] As in the case of the monoclinic form, some side chains and several short segments of the

https://dx.doi.org/10.1021/acsinfecdis.9b00368
ACS Infect. Dis. XXXX, XXX, XXX−XXX

protein (mainly loops 69-TGHL-72, 110-GIGKK-114 and less frequently 129-SGGP-132) were not clearly visible in most electron density maps or showed alternating configurations. Similarly, the last residue and/or the affinity-tag could not be modeled in most protein−ligand complexes. Figures of ligands and corresponding electronic density were generated using PyMOL (http://pymol.sourceforge.net). Refinement statistics are provided in Tables S1−S10.

Database Accession Codes. The refined models and structure factors have been deposited in the Research Collaboratory for Structural Biology (http://www.rcsb.org) under the following PDB accession numbers: 6RBO, 6RBP, 6RBQ, 6RR2, 6RBR, 6RBS, 6RBT, 6RBU, 6RBV, 6RBW, 6RBX, 6RBY, 6RBZ, 6RC0, 6RC1, 6RC2, 6RC3, 6RC4, 6RC5, 6RC6, 6RG6, 6RG7, 6RG8, 6RG9, 6RGA, 6RGB, 6RGC, 6RGD.

Bacterial Strains and Culture Conditions. *Staphylococcus aureus* Xen36 and Xen31 were obtained from Caliper Life Science. Xen36 was derived from a clinical strain isolated from a bacteremic patient (ATCC 49525). Xen31 was derived from a clinical MRSA isolated in Elmhurst Hospital in New York (ATCC 33591). *Staphylococcus aureus* RN4220 is a restriction-deficient laboratory strain widely used for cloning (ATCC 35556). *S. aureus* strains were grown in Brain Heart Infusion (BHI) broth (BD) with shaking at 200 rpm or on BHI agar plates at 37 °C. *Escherichia coli* TOP10 were obtained from Invitrogen and grown in LB broth with shaking at 200 rpm or on LB agar plates at 37 °C. When required, culture medium was supplemented with antibiotics (carbenicillin 100 μg/mL for *E. coli*, chloramphenicol 15 μg/mL, anhydrotetracyclin 100 ng/mL for *S. aureus*).

Construction of the *ppnK* Knockdown Plasmid. The plasmid pSD1 was a gift from Changlong Zhao.[18] The two primers ppnK-sgRNA-oligo1 (CTAATTGTTATTTCAGTTGGTGGTGA) and ppnK-sgRNA-oligo2 (AACTCACCACCAACTGAAATAACAAT) were used as sgRNA. They were annealed and cloned into *Sap*I-digested pSD1, resulting in plasmid pOD134 (NADK sgRNA). *E. coli* TOP10 was transformed with pOD134, creating strain OD336.

Preparation of Electrocompetent *S. aureus*. Five milliliters of BHI broth were inoculated with a single colony of *S. aureus* and incubated at 37 °C and 200 rpm overnight. One milliliter of the overnight culture was added to 100 mL of BHI broth and shaken at 200 rpm at 37 °C until an optical density at 600 nm of 0.4 was reached. After 5 min on ice, the culture was centrifuged at 2500*g* for 10 min at 4 °C. The supernatant was discarded and bacteria were resuspended in 10 mL of ice-cold 0.5 M sucrose. Centrifugation and resuspension steps were repeated twice. Bacteria were then resuspended in 1 mL of ice-cold 0.5 M sucrose, kept on ice for 15 min, and divided in 100 μL aliquots. Electrocompetent bacteria were stored at −80 °C.

Transformation in *S. aureus*. Purified pOD134 or pSD1 was introduced into *S aureus* RN4220 and subsequently in *S. aureus* Xen36. Plasmid DNA (200 to 500 ng) and electrocompetent *S. aureus* (100 μL) were mixed and transferred in a 0.2 cm gap-cuvette (Molecular Bioproduct). Strains were transformed by electroporation at 2.5 kV using a Biorad Micro-Pulser. Immediately after electroporation, 500 μL of BHI were added to the cuvette and bacteria were incubated at 37 °C for 1 h with shaking at 200 rpm before plating on BHI agar supplemented with chloramphenicol (7 μg/mL). Plates were incubated overnight at 37 °C.

Plasmid Isolation and Purification from *S. aureus*. Plasmids were isolated from *S. aureus* using the QIAprep Spin Miniprep Kit (Qiagen) according to the manufacturer's instructions after a cell digestion step with 0.5 mg/mL of lysostaphine (Sigma-Aldrich) for 30 min at 37 °C.

Bacterial Growth Measurement. Overnight *S. aureus* cultures in BHI at 37 °C were diluted 1:100 into BHI broth. For NADK inhibition experiments, culture medium was supplemented with 0 to 100 ng/mL anhydrotetracycline (Sigma-Aldrich) and 25 μg/mL chloramphenicol when required. For antibiotic activity assay, culture medium was supplemented with 25% PBS/10% DMSO, 0.01 μg/mL NKI1 in 25% PBS/10% DMSO or 10 μg/mL levofloxacin. Cultures were incubated in 96-well plates or in Erlenmeyer, with shaking at 200 rpm at 37 °C. Growth was monitored with a microplate reader (Glomax Discover, Promega). Experiments were performed at least three times.

Immunoblotting. Bacteria grown for 3 or 6 h were collected by centrifugation 10 min at 10 000 rpm at 4 °C and resuspended in 500 μL of PBS. Bacteria were lysed by 6 cycles of 10-s sonication and 10-s rest on ice. Lysates were centrifuged for 15 min at 10 000 rpm at 4 °C and supernatants collected for protein quantification using the Qubit Protein Assay (Invitrogen). Samples were mixed with Laemmli buffer (Biorad) and 10% β-mercaptoethanol and denatured for 5 min at 95 °C. Samples were separated onto 4−20% MiniProtean TGX Stain-Free Precast Gel (Biorad) in TGS buffer and transferred on polyvinylidene fluoride membranes. Membranes were incubated overnight at 4 °C with primary antibodies diluted in 5% blotto (R114 rabbit anti-EF-Tu polyclonal antibodies, 1:5000; R250 rabbit polyclonal anti-*S. aureus* NADK antibodies, 1:1000). Membranes were then incubated with 1:2500 antirabbit horseradish peroxidase-conjugated antibodies (Abcam). Blots were revealed using the ECL kit (Pierce).

NADP(H)/NAD(H) Quantitation. Levels of NAD(H) and NADP(H) were assessed by using the NAD/NADH-Glo assay (Promega) and NADP/NADPH-Glo assay (Promega), respectively. Briefly, bacteria were grown 6 h at 37 °C and 180 rpm. Growth was stopped by addition of 100 μL of reconstituted detection reagent to 100 μL of bacterial suspension. Samples were incubated for 45 min at room temperature and bioluminescence was measured on a GloMax Discover plate reader. Bioluminescence signal was normalized to OD_{600nm}.

Cytotoxicity Assay. Increasing concentrations of diadenosine derivatives were added to MRC-5 human fetal lung fibroblasts for 3 days and cell viability was assayed using a quantitative metabolic assay with MTT (3-(4,5-dimethylthiazol-2-yl)-2,5-diphenyltetrazolium bromide) by the Imagif platform (Institut de Chimie des Substances Naturelles Gif-sur-Yvette, France). Measurements were performed in triplicate with a Biomek workstation (Beckman) in 96-well plates.

Metabolic Stability. A microsomal stability assay to measure *in vitro* intrinsic clearance and identify putative metabolites formed was performed by the TechMed platform (ESBS, Strasbourg, France). Briefly, 1 μM NKI1 was incubated at 37 °C with human liver microsomes (0.5 mg/mL) containing 1 mM NADPH and 3 mM $MgCl_2$. Samples were taken every 15 min and enzymatic reactions were stopped by addition of acetonitrile at 0 °C. The percentage of remaining NKI1 was determined by LC-MS/MS by measuring the area

https://dx.doi.org/10.1021/acsinfecdis.9b00368
ACS Infect. Dis. XXXX, XXX, XXX−XXX

under the peak of the compound on the chromatogram. Testosterone was used as positive control.

***In Vitro* Plasma Stability.** Plasma stability was performed by the TechMed platform (ESBS, Strasbourg, France). Briefly, 1 μM NKI1 was incubated at 37 °C with CD-1 mice plasma (400 μL). After 30 min incubation, samples (70 μL) were taken every 15 min and reactions were stopped by addition of acetonitrile (175 μL) at 0 °C. Samples were then sonicated and centrifuged for 5 min at 4 °C, and the supernatants analyzed by LC-MS/MS. The percentage of remaining NKI1 was determined by measuring the area under the peak of the compound on the chromatogram. Parocaïne was used as positive control.

Mouse Plasma Biochemical Parameters. Eight-week-old female BALB/c mice (Charles River) housed under specific-pathogen-free conditions received food and water ad libitum. Mice were treated daily intraperitoneally with PBS/10% DMSO or 2 mg NKI1 in PBS/10% DMSO over 7 days. Mouse weight was monitored every day. Blood was collected after 7 days of treatment for quantitation of urea, creatinine, alanine aminotransferase (ALT), and aspartate aminotransferase (AST) using Reflotron strips (Roche) with Reflovet (Scil). The kidneys were collected aseptically after 7 days for histological analysis.

Mouse Infection Model. Eight-week-old female BALB/c mice (Charles River) housed under specific-pathogen-free conditions received food and water ad libitum and their weight was recorded every day throughout the duration of the experiment. Mice were infected intravenously with 5×10^7 bacteria for the Xen36 strain or 10^7 bacteria for the Xen31 strain. Mice were sacrificed 7 days postinfection. Kidneys were dissected under aseptic conditions for bacteriological and histological analysis. The number of CFU was determined by plating serial dilutions of organ homogenates on BHI agar.

Mouse Histology. During necropsy, the kidneys were removed, immediately fixed in 10% neutral-buffered formalin for 1 week and embedded in paraffin. Transverse 4 μm-thick sections were cut for one kidney and longitudinal sections for the other. For a low number of mice, the papilla was incompletely or not observed on the longitudinal section because of the section orientation. Sections were stained in hematoxylin/eosin. Bacteria were highlighted using Gram stain.

Statistical Analysis. Results are expressed as means ± SEM of at least 3 replicates. Statistical analysis was performed using GraphPad Prism (GraphPad Software). Student's *t*-test (two-tailed) or two-way ANOVA were used to compare data. Differences between groups were considered significant when the *p* value was lower than 0.05.

Ethical Statement. All experiments were performed according to the French national and European laws and conformed to the European Council Directive on the approximation of laws, regulations, and administrative provisions of the Member States regarding the protection of animals used for experimental and other scientific purposes (86/609/EEC). The experimental procedures were approved by the Animal Experiment Committee and the Risk Prevention Service of the Institut Pasteur (approval numbers 160118 and 18−191).

■ ASSOCIATED CONTENT

Supporting Information

The Supporting Information is available free of charge at https://pubs.acs.org/doi/10.1021/acsinfecdis.9b00368.

Supplementary Figures S1−S13 and Tables S1−S10; General consideration, experimental procedures for synthesized library and diadenosine derivatives, including Schemes S1−S8, characterization data, and NMR spectra for compounds used in this study (PDF)

■ AUTHOR INFORMATION

Corresponding Authors

Sylvie Pochet − *Unité de Chimie et Biocatalyse, Institut Pasteur, CNRS UMR3523, 75015 Paris, France*; orcid.org/0000-0002-7774-7861; Email: sylvie.pochet@pasteur.fr

Gilles Labesse − *Centre de Biochimie Structurale, CNRS UMR 5048, INSERM U1054, Université Montpellier, 34090 Montpellier, France*; Email: labesse@cbs.cnrs.fr

Olivier Dussurget − *Unité de Recherche Yersinia, Institut Pasteur, 75015 Paris, France; Université de Paris, Sorbonne Paris Cité, 75013 Paris, France*; Email: olivier.dussurget@pasteur.fr

Authors

Muriel Gelin − *Centre de Biochimie Structurale, CNRS UMR 5048, INSERM U1054, Université Montpellier, 34090 Montpellier, France*

Julie Paoletti − *Unité de Chimie et Biocatalyse, Institut Pasteur, CNRS UMR3523, 75015 Paris, France*

Marie-Anne Nahori − *Unité des Toxines Bactériennes, Institut Pasteur, 75015 Paris, France*

Valérie Huteau − *Unité de Chimie et Biocatalyse, Institut Pasteur, CNRS UMR3523, 75015 Paris, France*

Clarisse Leseigneur − *Unité de Recherche Yersinia, Institut Pasteur, 75015 Paris, France; Université de Paris, Sorbonne Paris Cité, 75013 Paris, France*

Grégory Jouvion − *Unité de Neuropathologie Expérimentale, Institut Pasteur, 75015 Paris, France; Sorbonne Université, INSERM UMR S933, Unité de Génétique Médicale, Hôpital Armand Trousseau, 75012 Paris, France*

Laurence Dugué − *Unité de Chimie et Biocatalyse, Institut Pasteur, CNRS UMR3523, 75015 Paris, France*

David Clément − *Unité de Chimie et Biocatalyse, Institut Pasteur, CNRS UMR3523, 75015 Paris, France; Université de Paris, Sorbonne Paris Cité, 75013 Paris, France*

Jean-Luc Pons − *Centre de Biochimie Structurale, CNRS UMR 5048, INSERM U1054, Université Montpellier, 34090 Montpellier, France*

Liliane Assairi − *INSERM U759, Institut Curie, Centre Universitaire Paris Sud, 91405 Orsay, France*

Complete contact information is available at: https://pubs.acs.org/10.1021/acsinfecdis.9b00368

Author Contributions

[¶]M.G., J.P., M.-A.N., and V.H. contributed equally to this work. M.G. performed crystallogenesis and ligand screening. M.G. and G.L. refined crystal structures. L.A. performed protein purification and biochemical studies. J.P., V.H., L.D., and D.C. performed chemical synthesis. C.L. generated bacterial strains. M.A.N. and C.L. performed bacterial experiments *in vitro*. M.A.N., C.L., and O.D. performed *in vivo* experiments. G.J. performed the histological experiments

https://dx.doi.org/10.1021/acsinfecdis.9b00368
ACS Infect. Dis. XXXX, XXX, XXX−XXX

and analyzed the data. O.D., S.P., and G.L. coordinated the study, interpreted the data, and wrote the paper.

Notes

The authors declare no competing financial interest.

■ ACKNOWLEDGMENTS

We thank Dr. Changlong Zhao for providing the plasmid pSD1. We wish to acknowledge Dr. Cécile Gasse, Dr. Laurence Morelatto, and William Pauly-Batard for their contribution to the preparation of adenine derivatives; Frédéric Bonhomme for assisting with HRMS analysis; the TechMed platform (ESBS, Strasbourg, France) for providing compound stability data; and the Imagif platform (Institut de Chimie des Substances Naturelles, Gif-sur-Yvette, France) for assistance with cytotoxicity assays. We thank Dr. Jean-François Guichou, Dr. Martin Cohen-Gonsaud for helpful discussions and technical help. This work was supported by the Agence Nationale de la Recherche (grants ANR-06-BLAN-0324, ANR-11-EMM-0019, and ANR-17-CE18-0011-02), the Centre National de la Recherche Scientifique (CNRS), Institut National de la Santé et de la Recherche Médicale (INSERM), Institut Pasteur and Institut Curie. DC and CL acknowledge ANR for financial support (ANR-17-CE18-0011-02). We also acknowledge support from the French Infrastructure for Integrated Structural Biology (FRISBI) ANR-10-INSB-05-01 and Idex UP2019. We thank the staff of ESRF and of EMBL-Grenoble for assistance and support in using beamlines ID14-1, ID14-4, ID23-1, ID23-2, ID29, ID30B, ID30A1, and ID30A3.

■ ABBREVIATIONS

ATc, anhydro-tetracycline; BHI, brain heart infusion; Cas9, CRISPR associated protein 9; CRISPR, clustered regularly interspaced short palindromic repeats; DMSO, dimethyl sulfoxide; FBDD, fragment-based drug design; LC-MS/MS, liquid chromatography−tandem mass spectrometry; MRSA, methicillin-resistant *Staphylococcus aureus*; NAD, nicotinamide adenine dinucleotide; NADH, reduced form of NAD; NADK, nicotinamide adenine dinucleotide kinase; NADP, nicotinamide adenine dinucleotide phosphate; NADPH, reduced form of NADP; NKI1, NAD kinase inhibitor 1; NMR, nuclear magnetic resonance; OD, optical density; PBS, phosphate buffered saline; sgRNA, single guide RNA.

■ REFERENCES

(1) Fischbach, M. A., and Walsh, C. T. (2009) Antibiotics for emerging pathogens. *Science 325*, 1089−1093.

(2) McGuinness, E. T., and Butler, J. R. (1985) NAD+ kinase−a review. *Int. J. Biochem. 17*, 1−11.

(3) Kawai, S., Mori, S., Mukai, T., Suzuki, S., Yamada, T., Hashimoto, W., and Murata, K. (2000) Inorganic polyphosphate/ATP-NAD kinase of *Micrococcus flavus* and *Mycobacterium tuberculosis* H37Rv. *Biochem. Biophys. Res. Commun. 276*, 57−63.

(4) Gerdes, S. Y., Scholle, M. D., D'Souza, M., Bernal, A., Baev, M. V., Farrell, M., Kurnasov, O. V., Daugherty, M. D., Mseeh, F., Polanuyer, B. M., Campbell, J. W., Anantha, S., Shatalin, K. Y., Chowdhury, S. A. K., Fonstein, M. Y., and Osterman, A. L. (2002) From Genetic Footprinting to Antimicrobial Drug Targets: Examples in Cofactor Biosynthetic Pathways. *J. Bacteriol. 184* (16), 4555−4572.

(5) Kobayashi, K., Ehrlich, S. D., Albertini, A., Amati, G., Andersen, K. K., Arnaud, M., Asai, K., Ashikaga, S., Aymerich, S., Bessieres, P., Boland, F., Brignell, S. C., Bron, S., Bunai, K., Chapuis, J., Christiansen, L. C., Danchin, A., Débarbouillé, M., Dervyn, E., Deuerling, E., Devine, K., Devine, S. K., Dreesen, O., Errington, J., Fillinger, S., Foster, S. J., Fujita, Y., Galizzi, A., Gardan, R., Eschevins, C., Fukushima, T., Haga, K., Harwood, C. R., Hecker, M., Hosoya, D., Hullo, M. F., Kakeshita, H., Karamata, D., Kasahara, Y., Kawamura, F., Koga, K., Koski, P., Kuwana, R., Imamura, D., Ishimaru, M., Ishikawa, S., Ishio, I., Le Coq, D., Masson, A., Mauël, C., Meima, R., Mellado, R. P., Moir, A., Moriya, S., Nagakawa, E., Nanamiya, H., Nakai, S., Nygaard, P., Ogura, M., Ohanan, T., O'Reilly, M., O'Rourke, M., Pragai, Z., Pooley, H. M., Rapoport, G., Rawlins, J. P., Rivas, L. A., Rivolta, C., Sadaie, A., Sadaie, Y., Sarvas, M., Sato, T., Saxild, H. H., Scanlan, E., Schumann, W., Seegers, J. F. M. L., Sekiguchi, J., Sekowska, A., Séror, S. J., Simon, M., Stragier, P., Studer, R., Takamatsu, H., Tanaka, T., Takeuchi, M., Thomaides, H. B., Vagner, V., van Dijl, J. M., Watabe, K., Wipat, A., Yamamoto, H., Yamamoto, M., Yamamoto, Y., Yamane, K., Yata, K., Yoshida, K., Yoshikawa, H., Zuber, U., and Ogasawara, N. (2003) Essential *Bacillus subtilis* genes. *Proc. Natl. Acad. Sci. U. S. A. 100*, 4678−4683.

(6) Sassetti, C. M., Boyd, D. H., and Rubin, E. J. (2003) Genes required for mycobacterial growth defined by high density mutagenesis. *Mol. Microbiol. 48*, 77−84.

(7) Labesse, G., Douguet, D., Assairi, L., and Gilles, A. M. (2002) Diacylglyceride kinases, sphingosine kinases and NAD kinases: distant relatives of 6-phosphofructokinases. *Trends Biochem. Sci. 27*, 273−275.

(8) Petrelli, R., Sham, Y. Y., Chen, L., Felczak, K., Bennett, E., Wilson, D., Aldrich, C., Yu, J. S., Cappellacci, L., Franchetti, P., Grifantini, M., Mazzola, F., Di Stefano, M., Magni, G., and Pankiewicz, K. W. (2009) Selective inhibition of nicotinamide adenine dinucleotide kinases by dinucleoside disulfide mimics of nicotinamide adenine dinucleotide analogues. *Bioorg. Med. Chem. 17*, 5656−5664.

(9) Schulz, M. N., and Hubbard, R. E. (2009) Recent progress in fragment-based lead discovery. *Curr. Opin. Pharmacol. 9*, 615−621.

(10) Erlanson, D. A., Fesik, S. W., Hubbard, R. E., Jahnke, W., and Jhoti, H. (2016) Twenty years on: the impact of fragments on drug discovery. *Nat. Rev. Drug Discovery 15*, 605−619.

(11) Shuker, S. B., Hajduk, P. J., Meadows, R. P., and Fesik, S. W. (1996) Discovering high-affinity ligands for proteins: SAR by NMR. *Science 274*, 1531−1534.

(12) Howard, N., Abell, C., Blakemore, W., Chessari, G., Congreve, M., Howard, S., Jhoti, H., Murray, C. W., Seavers, L. C. A., and van Montfort, R. L. M. (2006) Application of fragment screening and fragment linking to the discovery of novel thrombin inhibitors. *J. Med. Chem. 49*, 1346−1355.

(13) Hung, A. W., Silvestre, H. L., Wen, S., Ciulli, A., Blundell, T. L., and Abell, C. (2009) Application of fragment growing and fragment linking to the discovery of inhibitors of *Mycobacterium tuberculosis* pantothenate synthetase. *Angew. Chem., Int. Ed. 48*, 8452−8456.

(14) Jencks, W. P. (1981) On the attribution and additivity of binding energies. *Proc. Natl. Acad. Sci. U. S. A. 78*, 4046−4050.

(15) Poncet-Montange, G., Assairi, L., Arold, S., Pochet, S., and Labesse, G. (2007) NAD kinases use substrate-assisted catalysis for specific recognition of NAD. *J. Biol. Chem. 282*, 33925−34.

(16) Gelin, M., Poncet-Montange, G., Assairi, L., Morellato, L., Huteau, V., Dugué, L., Dussurget, O., Pochet, S., and Labesse, G. (2012) Screening and *in situ* synthesis using crystals of a NAD kinase lead to a potent antistaphylococcal compound. *Structure 20*, 1107−1117.

(17) Paoletti, J., Assairi, L., Gelin, M., Huteau, V., Nahori, M. A., Dussurget, O., Labesse, G., and Pochet, S. (2016) 8-Thioalkyl-adenosine derivatives inhibit *Listeria monocytogenes* NAD kinase through a novel binding mode. *Eur. J. Med. Chem. 124*, 1041−1056.

(18) Zhao, C., Shu, X., and Sun, B. (2017) Construction of a gene knockdown system based on catalytically inactive ('Dead') Cas9 (dCas9) in *Staphylococcus aureus*. *Appl. Environ. Microbiol. 83*, 2026−2015.

(19) Ji, Y., Zhang, B., Van, S. F., Horn, Warren, P., Woodnutt, G., Burnham, M. K., and Rosenberg, M. (2001) Identification of critical staphylococcal genes using conditional phenotypes generated by antisense RNA. *Science 293*, 2266−2269.

(20) Forsyth, R. A., Haselbeck, R. J., Ohlsen, K. L., Yamamoto, R. T., Xu, H., Trawick, J. D., Wall, D., Wang, L., Brown-Driver, V., Froelich, J. M., C, K. G., King, P., McCarthy, M., Malone, C., Misiner, B.,

https://dx.doi.org/10.1021/acsinfecdis.9b00368
ACS Infect. Dis. XXXX, XXX, XXX−XXX

970 Robbins, D., Tan, Z., Zhu Zy, Z. Y., Carr, G., Mosca, D. A., Zamudio,
971 C., Foulkes, J. G., and Zyskind, J. W. (2002) A genome-wide strategy
972 for the identification of essential genes in *Staphylococcus aureus*. *Mol.*
973 *Microbiol. 43*, 1387−1400.
974 (21) Bae, T., Banger, A. K., Wallace, A., Glass, E. M., Åslund, F.,
975 Schneewind, O., and Missiakas, D. M. (2004) *Staphylococcus aureus*
976 virulence genes identified by *bursa aurealis* mutagenesis and nematode
977 killing. *Proc. Natl. Acad. Sci. U. S. A. 101*, 12312−12317.
978 (22) Chaudhuri, R. R., Allen, A. G., Owen, P. J., Shalom, G., Stone,
979 K., Harrison, M., Burgis, T. A., Lockyer, M., Garcia-Lara, J., Foster, S.
980 J., Pleasance, S. J., Peters, S. E., Maskell, D. J., and Charles, I. G.
981 (2009) Comprehensive identification of essential *Staphylococcus*
982 *aureus* genes using Transposon-Mediated Differential Hybridisation
983 (TMDH). *BMC Genomics 10*, 291−218.
984 (23) Yamachika, S., Onodera, Y., Hiramatsu, K., and Takase, H.
985 (2012) Plasmid integration method: a new tool for analysis of the
986 essentiality and function of genes in *S. aureus*. *J. Microbiol. Methods 90*,
987 250−255.
988 (24) Lowy, F. D. (1998) *Staphylococcus aureus* infections. *N. Engl. J.*
989 *Med. 339*, 520−532.
990 (25) Tarkowski, A., Collins, L. V., Gjertsson, I., Hultgren, O. H.,
991 Jonsson, I.-M., Sakiniene, E., and Verdrengh, M. (2001) Model
992 systems: modeling human staphylococcal arthritis and sepsis in the
993 mouse. *Trends Microbiol. 9*, 321−326.
994 (26) Yu, J., Wu, J., Francis, K. P., Purchio, T. F., and Kadurugamuwa,
995 J. L. (2005) Monitoring *in vivo* fitness of rifampicin-resistant
996 *Staphylococcus aureus* mutants in a mouse biofilm infection model. *J.*
997 *Antimicrob. Chemother. 55*, 528−534.
998 (27) Kugelberg, E., Norstrom, T., Petersen, T. K., Duvold, T.,
999 Andersson, D. I., and Hughes, D. (2005) Establishment of a
1000 superficial skin infection model in mice by using *Staphylococcus*
1001 *aureus* and *Streptococcus pyogenes*. *Antimicrob. Agents Chemother. 49*,
1002 3435−3441.
1003 (28) Kim, H. K., Missiakas, D., and Schneewind, O. (2014) Mouse
1004 models for infectious diseases caused by *Staphylococcus aureus*. *J.*
1005 *Immunol. Methods 410*, 88−99.
1006 (29) Fernandes, P. B., and Swanson, R. N. (1998) Correlation of *in*
1007 *vitro* activities of the fluoroquinolones to their *in vivo* efficacies. *Drugs*
1008 *Exp. Clin. Res. 14*, 375−378.
1009 (30) Frosco, M. B., Melton, J. L., Stewart, F. P., Kulwich, B. A.,
1010 Licata, L., and Barrett, J. F. (1996) *In vivo* efficacies of levofloxacin
1011 and ciprofloxacin in acute murine hematogenous pyelonephritis
1012 induced by methicillin-susceptible and-resistant *Staphylococcus aureus*
1013 strains. *Antimicrob. Agents Chemother. 40*, 2529−2534.
1014 (31) Peterson, J., Kaul, S., Khashab, M., Fisher, A. C., and Kahn, J. B.
1015 (2008) A double-blind, randomized comparison of levofloxacin 750
1016 mg once-daily for five days with ciprofloxacin 400/500 mg twice-daily
1017 for 10 days for the treatment of complicated urinary tract infections
1018 and acute pyelonephritis. *Urology 71*, 17−22.
1019 (32) Noel, G. J. (2009) A review of levofloxacin for the treatment of
1020 bacterial Infections. *Clin. Med.: Therapeutics 1*, 433−458.
1021 (33) Schaefler, S., Perry, W., and Jones, D. (1979) D. Methicillin-
1022 resistant strains of *Staphylococcus aureus* Phage Type 92. *Antimicrob.*
1023 *Agents Chemother. 15*, 74−80.
1024 (34) Adams, P. D., Afonine, P. V., Bunkoczi, G., Chen, V. B., Davis,
1025 I. W., Echols, N., Headd, J. J., Hung, L. W., Kapral, G. J., Grosse-
1026 Kunstleve, R. W., McCoy, A. J., Moriarty, N. W., Oeffner, R., Read, R.
1027 J., Richardson, D. C., Richardson, J. S., Terwilliger, T. C., and Zwart,
1028 P. H. (2010) PHENIX: a comprehensive Python-based system for
1029 macromolecular structure solution. *Acta Crystallogr., Sect. D: Biol.*
1030 *Crystallogr. 66*, 213−221.

https://dx.doi.org/10.1021/acsinfecdis.9b00368
ACS Infect. Dis. XXXX, XXX, XXX−XXX